This is a repository copy of *Laboratory Experiment on the Control of Distillation Column Pressure by Microprocessor*.

White Rose Research Online URL for this paper:
http://eprints.whiterose.ac.uk/76046/

Monograph:
Edwards, J.B. (1980) Laboratory Experiment on the Control of Distillation Column Pressure by Microprocessor. Research Report. ACSE Report 145A . Department of Control Engineering, University of Sheffield, Mappin Street, Sheffield

eprints@whiterose.ac.uk
https://eprints.whiterose.ac.uk/

A SYSTEMS ENGINEERING APPROACH TO THE DESIGN

AND TESTING OF BATTERY VEHICLE DRIVES

J.B. Edwards[*], M.Sc., B.Sc.(Eng.), C. Eng., M.I.E.E.

K. Pacey[†], Ph.D., B.Sc., A.M.I.E.E.

March 1980

[*] Senior Lecturer, Department of Control Engineering,
University of Sheffield

[†] Project Engineer, Chloride Legg Ltd., (formerly with
Chloride Technical Ltd.

A SYSTEMS ENGINEERING APPROACH TO THE DESIGN

AND TESTING OF BATTERY VEHICLE DRIVES

by J.B. Edwards and K. Pacey

SYNOPSIS

The dynamic laboratory testing of prototype drives is discussed:
a minicomputer controlling load and drive simultaneously. The roles of
inverse Nyquist analysis, sampled-data systems analysis and computer
simulation in design and commissioning are examined.

Drive = means by which mechanical power is transmitted to a machine.

- 1 -

1. Introduction

An essential feature of a systematic approach to the development of drives for novel applications is the dynamic testing of potential prototype drives in the laboratory to permit their appraisal and short listing for possible field trials. The field testing of each and every drive candidate would in general be prohibitively expensive and controlled conditions for fair comparative tests would be very difficult to achieve. These problems are accute in the case of road vehicles where the installation costs of prototype drives are particularly high and road   traffic conditions highly variable and unrepeatable.

The development of a laboratory facility for dynamic testing itself poses a number of control problems calling for control systems design techniques and computer simulation for their solution prior to the development of software for the computer control of the drive and test facility. Computer simulation and stability analysis have also been found to play an important role in the development of the various drives themselves and in the commisioning of the composite system.

The paper describes some of these aspects of research and development undertaken in this area collaboratively by Chloride   Technical and the Department of Control Engineering of the University of Sheffield.

2. The computer controlled test facility

There are two essential requirements for a proper comparison of the performance of a variety of vehicle drives on the test bed. These are that the drives should be:

(i) subjected to load patterns representative of identical and typical journeys as regards gradient profile, payload variation and vehicle parameters, and

(ii) driven in a manner to ensure that simulated journeys are completed according to a prescribed schedule (except, of course, where

such a schedule is found to be impossible of attainment by a particular
drive without serious overstressing mechanically, electrically or thermally,
in which case the drive should be severely penalised in relation to its more
successful competitors).

In the case of battery vehicle drives, the fundamental index of
performance is naturally the ampere-hour utilisation of the available
battery capacity, or conversely, the range attained for a given battery
discharge. Motor temperature and commutation are also important however
in the overall assessment of drive performance.

From a consideration if (i) and (ii) above it is clear that two basic
control systems are required for dynamic drive testing, these being an
automatic load control system and, in the interests of repeatability, an
automatic driver.

2.1 The dynamometer

For loading purposes a thryistor controlled d.c. dynamometer was
obtained comprising d.c. generator, inverter and control gear. As shown
in Fig. 1 the dynamometer is equipped transducers for measurement of speed
acceleration and motor-shaft torque and a local analogue controller designed
to minimise the error

$$\tau_e = \tau_s - \tau_v \tag{1}$$

where τ_v is the tractive effort which would be demanded from the test motor
by the simulated vehicle and τ_s is the tractive effort measured at the motor
shaft. Now τ_v comprises five components:

the vehicle acceleration load, $\quad \tau_1(t) = M_v' \, \dot{v}(t) \tag{2}$

aerodynamic drag, $\quad \tau_2(t) = f|v(t)|v(t) \tag{3}$

rolling resistance, $\quad \tau_3(t) = a \text{ constant} \tag{4}$

gradient load, $\quad \tau_4(x) = W_v \alpha(x) \tag{5}$

and mechanical braking effort $\quad \tau_5(t)$

where $x(t)$ is distance travelled, and $v(t)$ the vehicle velocity given by

$$v(t) = \dot{x}(t) \tag{6}$$

M'_v is the total inertial mass of the vehicle including the effective inertial mass of the rotating parts - less motor, W_v is the total weight of the vehicle and f its aerodynamic drag coefficient. $\alpha(x)$ is the distance-dependent road gradient (uphill values being positive). Thus

$$\tau_v = \tau_1(t) + \tau_2(t) + \tau_3 + \tau_4(x) - \tau_5(t) \tag{7}$$

Components τ_1, τ_2 and τ_3 may be synthesised within the local analogue control system by proper presetting of the vehicle mass and drag coefficients but τ_4, being an arbitrary function of distance, must be injected from an external source as indicated in Fig. 1. τ_5 is likewise an arbitrary function (dependent on driver action) and must therefore be synthesised externally also.

2.2 Computer functions

A P.D.P. 8/E mini computer was provided for the calculation and production of the signal $\tau_4(x)$ and to provide the automatic driver function in addition to data logging and overall test supervision. As a second phase it was planned that the computer should take over the calculation of all five load components and exercise the closed-loop load-control function so permitting the decoupling of any interaction effects discovered between the driver and load control loops and allowing the distance modulation of parameters M'_v and W_v to simulate distance-varying payloads.

Rather than applying one or other of the various published "standard" speed/time duty cycles* as a reference for the automatic driver, it was thought preferable to record a series of actual road journeys by arranging for a light instrumented vehicle to chase the petrol or diesel-driven counterpart (bus, delivery van or private car) of the vehicle for which the prototype drive was intended. The speed record $v_r(t)$ could then be played

* e.g. the duty cycles of I.S.I., S.A.E. or I.E.C.

back into the automatic driver controller. Distance profile y(t) is simply
obtained by integration of the recorded velocity signal. A pendulum incli-
nometer is recorded simultaneously with the road velocity signal and the
road gradient profile $\alpha(t)$ synthesised off-line by subtraction of the acce-
leration component from the pendulum (obtained from the derivative of the
road tachometer signal). In this way tables of $v_r(i)$, $y(i)$ and $\alpha(i)$ are made
available for the control of the laboratory testing. Integer i denotes the
ith time step at which the signals are sampled, stored and accessed by the
on-line control system, i.e. sampling instants are given by

$$t = i\Delta T, \quad o \leqslant i \leqslant N \tag{8}$$

(ΔT is the sampling interval and $N\Delta T$ the total journey duration). Most d.c.
drives employ some form of armature or battery current feedback to back-off
the driver's throttle signal which may therefore be regarded as a current
demand signal. An automatic driver therefore needs to provide such a demand,
$I_d(t)$ from a D/A converter instead. The automatic driving policy adopted
was simple two-term control, viz.

$$I_d(t) = k_a \{v_r(t) - v(t)\} + k_b \{x_r(t) - x(t)\} \tag{9}$$

where $v_r(t)$ and $x_r(t)$ denote the state of the reference (i.e. road-test)
vehicle at time t, v(t) and x(t) being the velocity and position of the
actual drive under test at this instant. k_a and k_b are the preset propor-
tional and integral gains.

Control law (9) is simple in its implementation requiring merely the
computer clock to determine time t, a measurement of v(t) from the test-bed
tachometer (from which x(t) and $\dot{v}(t)$ are obtained by digital integration
and differentiation) and access to the pre-stored tables of $v_r(i)$ and $x_r(i)$
{set = y(i)}. The calculation of $\tau_4(x)$ for output to the dynamometer con-
troller (Fig. 1), is however a little more involved because of the inevitable
discrepancy between x(t) and $x_r(t)$ in general. Fig. 2 illustrates how τ_4
must be obtained by the controlling software.

Basically, when t = say, $n\Delta T$, having calculated x(n), it is necessary
to find the time $m\Delta T$ at which the reference vehicle was at this position
i.e. when

$$y(m) = x(n) \tag{10}$$

so that $\alpha(m)$ may be obtained from the $\alpha(i)$ table. To find m involves the scanning of the $y(i)$ table either side of $i = n$ until a $y(i)$ acceptably close to $x(n)$ is found. This means that, if control is not to be hindered by disc transfers, a suitably large block of the tables must be constantly held in core storage. The necessary block size is determined as follows: If $\Delta T = 0.1$ s and the likely distance lag is say, 10 vehicle lengths = 60m, then at an average speed of 15m/s the associated time delay between reference and test drive would be $60/15 = 4.0$s $\equiv 40$ samples. A safe block size should therefore be 100 samples in this case bearing in mind that the test vehicle may overtake the reference drive in a braking situation.

For production of mechanical braking torque $\tau_5(t)$ we must return to the computer's automatic driver function. Equation (9) will produce, (through the test motor dynamics), both forward and reverse tractive efforts in general, but $I_d(t)$ will be hard-limited by the driver's throttle end-stops to values $\pm I_m$ where I_m is the maximum safe current, i.e.

$$|I_d(t)| \leqslant I_m \tag{11}$$

Once electrical braking becomes insufficient, mechanical braking is needed so that an appropriate policy for the control of the simulated mechanical braking effort is

$$\left.\begin{array}{ll} \tau_5(t) = -k_c \{I_d(t) + I_m\} & , \quad I_d(t) \leqslant -I_m \\ \tau_5(t) = 0 & , \quad I_d(t) > -I_m \end{array}\right\} \tag{12}$$

where k_c is a gain determined by experiment. To cause the dynamometer to produce the desired mechanical braking effort, the signal applied externally to the dynamometer controller is therefore $\tau_4(x)$ (obtained from gradient tables as discussed above) <u>minus</u> $\tau_5(t)$ {calculated from equation (12)}. Fig. 3. illustrates the overall test configuration.

3. Auto-driver simulation

Simulation of the automatic driver was carried out on an AD4 hybrid computer in order to tune the parameters k_a, k_b, k_c and k_d and to validate the control strategy before attempting its implementation on the PDP 8/E. For this purpose vehicle equations (2) to (7) and control equations (9), (11) and (12) were simulated with error τ_e set to zero, by setting

$$\tau_s = \tau_v \tag{13}$$

The dynamometer was thus assumed to be perfectly controlled at this stage of the investigations. The drive selected for simulation was that intended for the initial test-bed trials, namely a separately-excited d.c. machine with solid-state adjustable-field and armature supply voltages $V_f(t)$ and $V(t)$ respectively. Somewhat idealised, the drive model interlinking current demand $I_d(t)$ and shaft torque $\tau_s(t)$ is as follows:

$$V = E + I R \tag{14}$$

where $I(t)$ is the armature current, R the armature circuit resistance and motor e.m.f $E(t)$ is given by

$$E = k_m I_f v \tag{15}$$

where k_m is a drive constant and field current $I_f(t)$ is governed by

$$V_f = I_f R_f + \dot{I}_f L_f \tag{16}$$

, R_f and L_f being the resistance and inductance of the field windings The manipulable voltages $V(t)$ and $V_f(t)$ are hard-limited such that

$$o \leqslant V \leqslant V_b \tag{17}$$

where V_b is the fixed battery voltage, and

$$|V_f| \leqslant V_{fm} \tag{18}$$

where V_{fm} is the maximum field voltage.

The closed-loop current feedback controller acts on $V(t)$ and $V_f(t)$ such that, if

$$I_e = I_d - I \tag{19}$$

then $V = k_v |I_e|$ and $V_f = \text{signum} (I_e) V_{fm}$, $k_v |I_e| \leqslant V_b$ (20)

$V = V_b$ and $\text{signum} (I_e) V_{fm} - V_f = k_f I_e$, $k_v |I_e| > V_b$ (21)

Motor pull $\tau_m (t)$ is produced through the interaction of I and the field

flux (assumed proportional to I_f) so that

$$\tau_m = k_m I_f I$$ (22)

and by subtracting the armature acceleration torque (translated into an

equivalent linear force) we get

$$\tau_s = \tau_m - M_m \dot{v}$$ (23)

where M_m is the motor's rotational inertia converted into an equivalent

translational mass.

With the addition of the set of drive equations (14) to (23) we have

a complete system description provided the parameter values are known.

Simulating the system on the hybrid computer produces results typified by

Fig. 4 which were obtained for a 75 kw drive powering a 6 tonne vehicle,

the current and voltage limits being $I_m = 500A$, $V_b = 180$ V and $V_{fm}/R_f = 25$ A,

the fully excited motor generating an e.m.f of 180v at 10 m.p.h. Electrical

parameters employed were $R_a = 75$ mΩ, $R_f = 6.5$ Ω, $L_f = 4.5$ H. The drive

inertia was assumed to be equivalent to 10% of that of the vehicle and

aerodynamic drag to absorb full motor effort at 47 m.p.h. Optimum controller

gains were found to be of the order of $k_a = 75$ A per m/s and $k_b = 15$ A per m

respectively producing maximum transient following errors of some seven or

eight vehicle lengths as indicated in Fig. 4 which was obtained for a simu-

lated uphill journey of constant 5% gradient. Such errors were automati-

cally reduced to some one or two vehicle lengths by the end of each journey

stage and on level roads following errors overall were found to be much

reduced.

The lack of available drive power is manifested by a long period of

chasing by the test drive after the reference vehicle has come to rest,

as evidenced by the result shown in Fig. 5 for a 10% uphill gradient and

the total unsuitability of a drive is indicated by its having no time
to stop between journey stages.

The computer simulation tests were subsequently enhanced to include the
sampling effect of the digital control system and the proposed sampling
frequency of 5 Hertz was found to be more than adequate, producing a
barely discernible degradation of the performance of the automatic driver.

The overall conclusion drawn from these preliminary simulation studies
is that the simple driver strategy (equation 9 and 12) should indeed ensure
that the test drive will follow the reference vehicle faithfully to
within a few vehicle lengths under all reasonable operating conditions.
In situations where serious following errors do develop, these appear to
be the result of inadequate drive power rather than a lack of driver
intelligence. The question of optimising the auto-driver strategy is
however, discussed by the present authors in a companion paper.[1]

The simulation tests (reported above) do not however guarantee the
success of the overall computer control system. This is because the
dynamometer has been implicitly assumed to behave ideally, loading the
drive in a manner identical to that of the simulated road vehicle. On
the actual test bed however, the motor loading is controlled by an addi-
tional control loop and the problem of dynamic interaction between the drive
and load-control loops, and its possible effect on system stability, demands
serious attention. The problem is investigated analytically in the following
section of the paper.

4. Interaction of the drive and load-control loops

A tool which has been highly developed and widely applied to the
investigation of the stability and response of linear interactive multi-
variable systems, and the design of controllers therefor, is the inverse
Nyquist array (I.N.A) technique of Rosenbrock[2]. Although many of the

drives (such as separately excited d.c. motors with field weakening,
series motors etc.) to be investigated for electric vehicles have non-
linear control characteristics these can usually be linearised to permit
the investigation of their small perturbation behaviour about selected
working conditions. It is therefore not a serious restriction to limit
our investigations here to fixed-field armature-controlled drives which
are substantially linear and therefore more conveniently presented. The
authors have in fact extended their investigations on the following lines,
to include a number of non-linear-drives without seriously affecting the
broad conclusions drawn from the linear system studies here reported.

4.1 The inverse transfer-function matrix (T.F.M)

The transfer-function matrix (T.F.M) of the multivariable system is
a prerequisite for application of the I.N.A method and may be readily
derived in this case from the drive vehicle and dynamometer equations.
There are

$$\tau_s = \tau_m - M_m \dot{v} = \tau_g + M_g \dot{v} \tag{24}$$

$$\tau_v = M'_v \dot{v} + \lambda v \tag{25}$$

and

$$\tau_e = \tau_s - \tau_v \tag{26}$$

where the symbols used earlier have their previous significance, τ_g is the
torque developed by the dynamometer generator-translated into linear trac-
tive effort and M_g is the rotational inertia of generator and flywheel
expressed as a translational mass. In comparing the original equations
(2 to 7) for the simulated vehicle drag τ_v with equation (25) it will be
noticed that the aerodynamic component has here been linearised by making
this a linear function of v with a quasi-constant drag coefficient λ. In
addition, the constant rolling resistance τ_3 has been dropped, having no
effect on stability as has gradient component τ_4 on the assumption that
gradient changes have insufficient frequency bandwidth to seriously affect
the control system response. The system inputs are chosen to be motor
effort τ_m and generator effort τ_g on the assumptions:

(a)   that the armature current controllers of both motor and generator are very tightly tuned, and

(b)   that τ_g is directly manipulable by rapid generator field current adjustment.

.The effect of assumption (b) is assessed later and assumption (a) is well justified   , there being minimal lag in the armatures of d.c. machines. Through the manipulation of τ_m and τ_g it is required to control the variables v (the speed) and τ_e (the dynamometer loading error). v of course is required to follow the moving reference $v_r(t)$ whilst τ_e is to be regulated as close to zero as possible. The system outputs chosen are therefore λv and τ_e. λv is chosen in preference to v in order to yield a dimensionless T.F.M. $\underline{G}(s)$ which after Laplace transformation of equations (24) to (26) and some manipulation may be obtained in the inverse form

$$\underline{G}^{*}(s) = \underline{G}^{-1}(s) = \begin{pmatrix} 1 + (T_1 + T_2)s & , & 1 \\ \\ 1 + T_2 s & , & 1 \end{pmatrix} \tag{27}$$

where

$$\begin{pmatrix} \lambda \tilde{v} \\ \\ \tilde{\tau}_e \end{pmatrix} = \underline{G}(s) \begin{pmatrix} \tilde{\tau}_m \\ \\ \tilde{\tau}_g \end{pmatrix} \tag{28}$$

and the time constants T_1 and T_2 are given by

$$T_1 = (M_g + M_m)/\lambda \tag{29}$$

and

$$T_2 = (M'_v - M_g)/\lambda \tag{30}$$

so that

$$T_1 + T_2 = (M'_v + M_m)/\lambda \tag{31}$$

$T_1 + T_2$ thus represents the inertial time constant of the simulated vehicle.

Fig. 6 is a block diagram of the open-loop (i.e. uncontrolled) system.

4.2 Application of the inverse Nyquist array

Now although in normal circumstances $M_v' > M_g$, so making $T_2 > 0$,

and hence

$$|g_{21}^*(j\omega)| < |g_{11}^*(j\omega)| \qquad (32)$$

the open-loop system is not diagonally dominant[2,3] since

$$|g_{12}^*(j\omega)| \nless |g_{22}^*(j\omega)| \quad , \ (=1.0) \qquad (33)$$

so that little can be deduced from the loci of the diagonal terms

$g_{11}^*(j\omega)$ and $q_{22}^*(j\omega)$ as to the shape of the inverse Nyquist loci of the

two control loops. In the hope that a simple static diagonal controller

of open-loop T.F.M, $K(s)$ will suffice as originally planned, where

$$K(s) = \begin{pmatrix} k_1 & , & 0 \\ & & \\ 0 & , & k_2 \end{pmatrix} \qquad (34)$$

such that the inverse open loop T.F.M. becomes $K^{-1}(s) \ G^*(s)$ and the

inverse closed loop T.F.M. becomes

$$H^*(s) = I + K^{-1}(s) \ G^*(s) \qquad (35)$$

then we deduce that

$$H^*(s) = \begin{pmatrix} 1 + \{1 + (T_1+T_2)s\}k_1^{-1} & , & k_1^{-1} \\ & & \\ (1+T_2 s)k_2^{-1} & , & 1+k_2^{-1} \end{pmatrix} \qquad (36)$$

The system $H^*(s)$ can clearly now be rendered diagonally dominant by choosing

relatively large values of driver and dynamometer loop gains k_1 and k_2,

(= 10.0 say) and Fig. 7a shows circles of radius $h_{21}^*(j\omega)$ for the

typical parameter values $T_1 = 2.0s$, $T_2 = 28.0s$ and $k_1 = k_2 = 10$ whilst

Fig. 7b shows element $h_{22}^*(j\omega)$ (a single point) with circular Gershgorin

band radius $h_{12}^*(j\omega)$. Again however, whilst the Gershgorin bands

clearly now exclude the origin giving diagonal dominance, the band around

$h_{11}^*(j\omega)$ is so wide as to be of little use in predicting the true shape of

the auto-driver locus which must lie in the Gershgorin band around $h_{11}^*(j\omega)$.

Narrower uncertainty bands known as the Ostrowski bands[2,3] for two-input two-output systems are obtained by plotting circles of radius $|h_{21}^{*}(j\omega)||h_{12}^{*}(j\omega)|/|h_{22}^{*}(j\omega)|$ centred on points on the locus of $h_{11}^{*}(j\omega)$, and circles of radius $|h_{12}^{*}(j\omega)||h_{21}^{*}(j\omega)|/|h_{11}^{*}(j\omega)|$ centred on points $h_{22}^{*}(j\omega)$. The Ostrowski bands for the automatic driver and dynamometer loops are shown in Fig.8. The first band is clearly much narrower than the Gershgorin band of Fig.7a and indeed is sufficiently narrow to deduce the satisfactory closed loop behaviour of the controller . In particular, the proximity of the auto-driver locus, as estimated from the Ostrowski band, to the unit M circle predicts a critically damped closed loop response and, as regards the dynamometer locus it is clear that, as gains k_1 and k_2 are increased, the locus shrinks towards the point 1.0 + j o which represents perfect closed loop behaviour with zero error and zero lag.

4.3 Direct calculation of the inverse Nyquist loci

Despite the fact that the I.N.A. technique has predicted very satisfactory behaviour from this multivariable control system its usefulness should not however be overemphasised because the compensator $\underline{K}(s)$ (diagonal in this case) was not synthesised by the I.N.A. technique but was chosen instead on intuitive grounds only. The subsequent analysis confirmed its suitability. Just as easily it is possible to calculate the true inverse Nyquist loci for the two loops, once the precompensator has been decided upon, so removing all uncertainty associated with the Gershgorin and Ostrowski bands. In the original design project in fact this direct approach was the one adopted by the authors and I.N.A. applied subsequently for purposes of double checking. This alternative approach is now outlined:

Calling the automatic driver control loop (1) and the dynamometer control loop (2) then the authors' direct approach is to evaluate the open-loop transfer-function $q_1(s)$ of loop (1) with loop (2) closed, i.e.

$$q_1(s) = k_1 \lambda \, \tilde{v}/\tilde{\tau}_m \quad , \quad (\tilde{\tau}_g = - k_2 \, \tilde{\tau}_e) \qquad (37)$$

and the open-loop transfer-function $q_2(s)$ of loop (2) with loop (1) closed, i.e.

$$q_2(s) = k_2 \, \tilde{\tau}_e / \tilde{\tau}_g \quad , \quad \{\tilde{\tau}_m = -k_1 \lambda \tilde{v}\} \tag{38}$$

and so predict the closed loop behaviour of each loop from the inverse Nyquist loci $q_1^{-1}(j\omega)$ and $q_2^{-1}(j\omega)$ without uncertainty. The inverse transfer functions are readily deduced from the block diagram of Fig. 9 giving

$$q_1^{-1}(s) = \frac{k_2 + \{T_1 + k_2(T_1 + T_2)\}s}{k_1(k_2+1)} \tag{39}$$

and

$$q_2^{-1}(s) = \frac{k_1(1+T_1 s)}{k_2(k_1+1)\{1+(T_1+T_2)s\}} \tag{40}$$

The closed-loop locus $1 + q_1^{-1}(j\omega)$ is therefore simply a vertical straight line the points on which are found, as expected, to lie entirely in the Ostrowski band of Fig. 8 if $T_2 > 0$ and clearly the larger the value of dynamometer gain k_2, the more independent of the dynamometer controller the automatic driver becomes. In particular, we deduce from (39) that

$$\underset{k_2 \to \infty}{\text{Lim}} \quad q_1^{-1}(s) = \{1 + (T_1 + T_2)s\}/k_1 \tag{41}$$

the R.H.S. of (41) being the transfer-function of the real (linearised) vehicle and drive. The locus of $1 + q_2^{-1}(j\omega)$ is a semi-circle centred on the real axis and again lying entirely in the Ostrowski band, if $T_2 > 0$ having extreme values

$$1 + q_2^{-1}(o) = 1 + k_1/\{k_2(k_1+1)\} \tag{42}$$

and $\qquad \underset{\omega \to \infty}{\text{Lim}} \quad \{1 + q_2^{-1}(j\omega)\} = 1 + k_1 T_1/\{k_2(T_1+T_2)(k_1+1)\} \tag{43}$

Thus as predicted by the I.N.A. method, increasing k_2 causes the entire locus to shrink towards the point $1.0 + j\,o$ i.e. towards ideal closed-loop performance.

The qualification that $T_2 > 0$ for the true system loci to lie within the Ostrowski bands corresponds to $M_v' > M_g$: as will normally be the case. If however, the generator and flywheel inertia were to exceed that of the simulated vehicle (i.e. $T_2 < 0$) then it is clear from (36) that $\underline{H}^*(s)$ is necessarily no longer/diagonally dominant and the INA approach fails whilst useful predictions can still be made using the direct approach outlined above.

4.4 Inclusion of generator field time constant

The model employed in Section 4 has so far assumed τ_g and τ_m to be directly manipulable. This is reasonable so far as the armature-controlled motor is concerned but the generator torque must generally be controlled by field adjustment involving an exponential inductive lag of time constant T_f. Although this can be reduced by local feedback techniques, some lag will nevertheless remain. To examine its effect therefore we must replace k_2 in the foregoing transfer-function expressions by $k_2/(1 + T_f s)$. The modified expressions for $q_1^{-1}(s)$ and $q_2^{-1}(s)$ become

$$q_1^{-1}(s) = \frac{k_2 + \{T_1 + k_2(T_1 + T_2)\}s + T_1 T_f s^2}{k_1(k_2 + 1 + T_f s)} \tag{44}$$

and
$$q_2^{-1}(s) = \frac{k_1(1 + T_1 s)(1 + T_f s)}{k_2(k_1 + 1)\{1 + (T_1 + T_2)s\}} \tag{45}$$

$q_1^{-1}(j\omega)$ is therefore asymptotic at $\omega = 0$ and ∞ to its previous straight line shape but exhibits some deflection towards the critical point of the complex plane at intermediate frequencies. The deflection is readily limited by setting the system gains suitably high however. As regards $q_2^{-1}(j\omega)$, the locus now climbs vertically as ω increases and since $T_1 + T_2 \gg T_f$ generally, any transient deflection into the second quadrant (i.e. towards the critical point) is very small. The presence of T_f does not therefore upset the stability of either control loop.

The predictions of Section 4.3 and 4.4 are confirmed by time domain simulation of the complete system (now including the dynamometer control loop).

5. Sampling effects on dynamometer control

As already mentioned in Section 3, hybrid simulations of the automatic driver revealed no problems when sampling was introduced into this loop to simulate digital control. Subsequent trials of the real system likewise showed no problems while ever control of the inertia loading was left to the local analogue dynamometer controller. In phase 2 of the project however, transference of the inertia load calculation to the PDP8/E computer resulted in severe oscillation in the load demand signal at sampling frequency, limited only by saturation of the D/A converter. Severe vibration of the mechanical system naturally resulted. Similar oscillations were subsequently revealed by the hybrid computer on introducing sampling to the dynamometer control loop simulation so indicating true instability rather than accentuation of transducer noise and pick-up from the chopper controllers by the digital "differentiation". An analysis of the sampled-data scheme using z-transform techniques was therefore carried out on the following lines:-

For simplicity only inertia loads are here considered. Using a backward finite difference approximation to differentiation we have that

$$\tau_v(t) = M_v'\{\hat{v}(t_i) - \hat{v}(t_i-T)\}, \quad t_i \leqslant t < t_i + T \quad (46)$$

where $\hat{v}(t)$ is the drive velocity signal fed into the digital computer, t_i denotes the i'th sampling instant and T is the sampling interval so that

$$t_i = iT \quad (47)$$

As we shall see, the preprocessing of the tachometer signal $v(t)$ by a first-order lag filter of small time constant T_L greatly improves controller performance so that we here assume that

$$\hat{v}(t) = v(t) - T_L D \hat{v}(t) \quad (48)$$

where $D \equiv d/dt$. The shaft torque measurement $\tau_s(t)$ is also sampled by

the compter so that

$$\tau_e(t) = \tau_s(t_i) - \tau_v(t) \quad , \quad t_i \leqslant t < t_i + T \tag{49}$$

and, again assuming proportional control of generator torque we have:

$$\tau_g(t) = - k_2 \quad \tau_e(t_i) \quad , \quad t_i \leqslant t < t_i + T \tag{50}$$

From the continuous machine equations (24) we also deduce that, if

$\tau_m = 0$ (being regarded as a fixed throttle setting and therefore having no

effect on stabilitv)

$$\dot{v}(t) = - \tau_g(t)/(M_m + M_g) \tag{51}$$

and

$$\tau_s(t) = \tau_g(t) \, M_m/(M_m + M_g) \tag{52}$$

The sampled-data system described by equations (46) to (52) is represented

in block diagram form in Fig. 10 which indicates the transfer functions of

the various continuous and discrete operations involved. Taking z-transforms$^{(5)}$

of the system and reduction of the diagram yields the open-loop z-transfer-

function:

$$\frac{\tilde{\tau}_g(z)}{\tilde{\tau}_e(z)} = \frac{k_2}{(M_m + M_g)} \left[\frac{z^2(M_m T) + z \{-a \, M_m \, T + M'_v \, T + (a-1)M'_v \, T_L\} - \{M'_v \, T \, a + M'_v \, T_L(a-1)\}}{T \, z(z - a)} \right] \tag{53}$$

$$\tag{54}$$

where $a = \exp(- T/T_L)$

Now if the filter is omitted i.e. $T_L = 0$ the z-transfer function reduces

to simply

$$\frac{\tilde{\tau}_g(z)}{\tilde{\tau}_e(z)} = \frac{k_2(M_m \, z + M'_v)}{(M_m + M_g) \, z} \tag{55}$$

yielding a pole at the origin of the z-plane and a zero at

$$z = - M'_v/M_m \tag{56}$$

i.e. well outside the unit circle under normal circulstances ($M'_v \gg M_m$).

For only very small gains k_2 therefore the closed-loop root moves outside

the region of stability so predicting the instability observed on test and

in simulation. If however we consider a non-zero T_L (>> T) then an additional pole is clearly introduced at z = a i.e. just inside the unit circle whilst the two real zeros of the system occupy positions given by

$$z = \left[-\{c-a + (a-1)c/b\} \pm \sqrt{\{c-a + (a-1)c/b\}^2 + 4c\{(a-1)/b + a\}} \right] /2 \qquad (57)$$

where $c = M_v'/M_m$ \qquad\qquad (58)

and $b = T/T_L$ \qquad\qquad (59)

so that if b << 1.0 \qquad\qquad (60)

the zero positions are given by

$$z \simeq (a \pm \sqrt{a^2 - 4cb})/2 \qquad (61)$$

so that provided cb is somewhat less than unity, i.e. provided

$$T_L/T > M_v'/M_m \qquad (62)$$

the zeros are kept within the unit circle of the z-plane so that the closed-loop system roots remain stable for all gain k_2. Simulation shows that this basic rule of thumb (62) seems to hold when aerodynamic drag and drive nonlinearities are introduced and stability was in fact restored to the digitally controlled dynamometer loop by inclusion of an appropriate lag T_L, as expected. Of course for very large ratios M_v'/M_m it may prove necessary to reduce the sampling interval T in order that lag T_L should not introduce a significant dynamic error into the dynamometer response.

5. Discussion and Conclusions

The application of systems engineering techniques has proved to be invaluable throughout this project the successful outcome of which is demonstrated by the test bed results illustrated in Fig. 11 obtained for the drive and control system simulated in Section 3. In some cases, (e.g. analysis and computer simulation of the automatic driver loop and the speed/torque loop interaction problem), such techniques have provided prior reassurance of the stability and accuracy of the proposed control locus so that the inevitable faults encountered in commisioning could be confidently attributed to temporary misbehaviour of system components (transducers, data

links, software etc.) rather than to an invalid system strategy.

Where faults did appear, portable hybrid computers connected to the real hardware were used to great advantage to simulate parts of the system (drive or digital computer) in order to locate the faults. Fault tracing would otherwise have proved to be extremely tedious due to the multiple closed loop actions involved and the prototype nature of all the equipment.

These computers were also used on occasions to temporarily replace parts of the prototype "in-vehicle" power controllers in order to localise faults therein which had escaped detection onthe test bench, many faults not appearing until the electrically noisy environment of the test bed was encountered.

The effect of sampling on inertia simulation was not predicted à priori having been omitted from the early simulations. Once the problem was discovered on the test bed in phase 2 of the project however, simulation quickly confirmed sampling to be the culprit and control theory rapidly generated a simple successful compensation technique.

Subsequent work related to this project has also involved the application of systems techniques at both extremes of the control hierarchy. Detailed simulation and analysis of the pulsed behaviour of series motor drives[6] have been successfully conducted at the plant level whilst optimal overall control strategies have been evaluated for driving series and separately excited drives with a view to minimising energy wastage. This latter problem is discussed by the authors in a companion paper.[1]

7. References

(1) Edwards J. B. and Pacey K:- 'An optimal control approach to energy minimisation in electric vehicles': Paper No. 7, Proc. of I.Mech.E. Conference on Systems Engineering in Land Transport. Sept. 1980.

(2) Rosenbrock, H.H.: 'Computer aided control system design', Academic Press,1974.

(3)   Owens, D.H.: 'Feedback and multivariable systems', Peter Peregrinus,

I.E.E. Control Engineering Series 7, 1978.

(4)   Paltikian, H.I.: 'Computer control of the testing of electric traction

drives', University of Sheffield, Dept. of Control Engineering, Ph.D. Thesis,

June 1978.

(5)   Shinners, S.M.: 'Control system design', John Wiley & Sons, Inc. 1964.

(6)   Edwards, J.B.: 'Simulation of a chopper controlled series motor drive

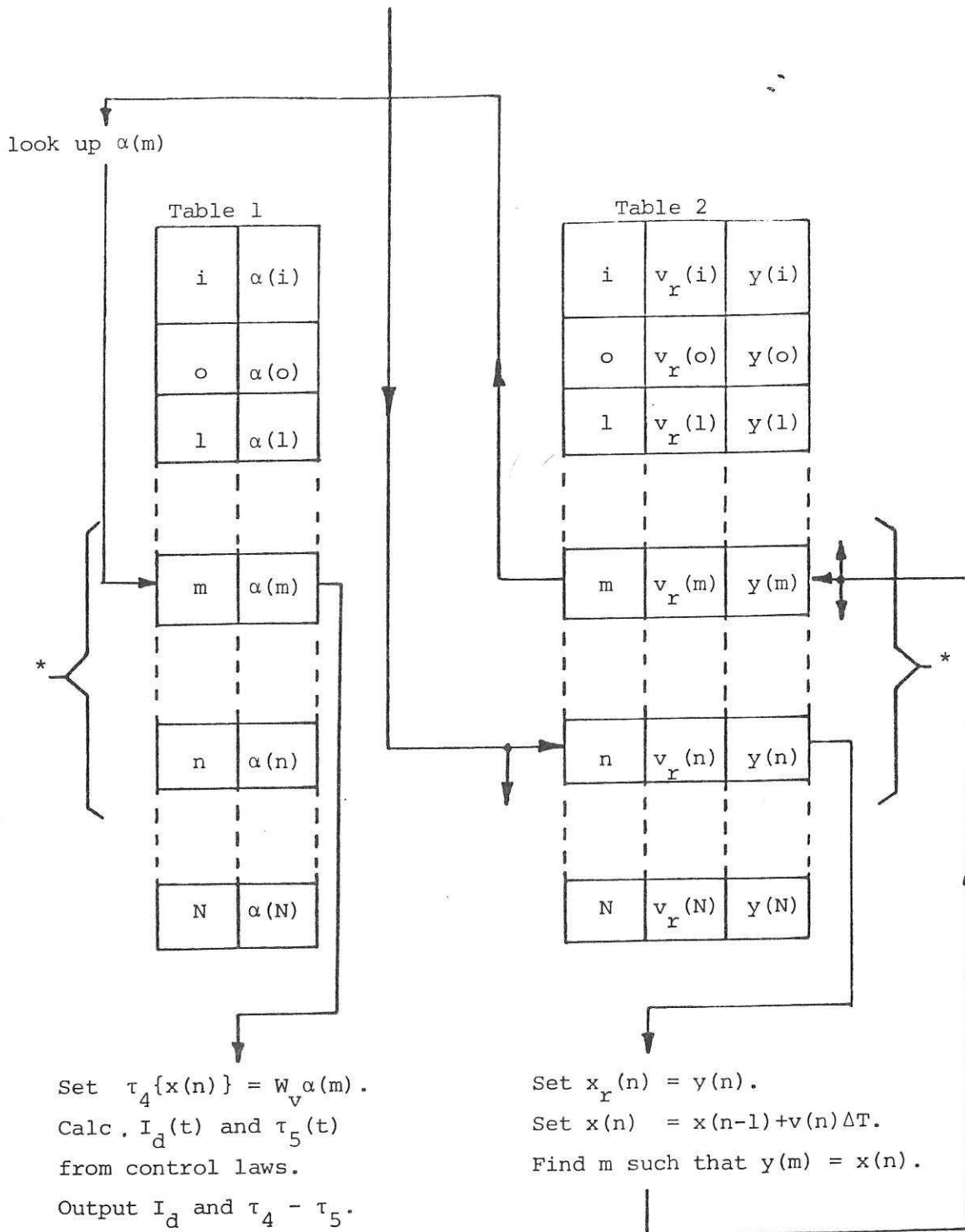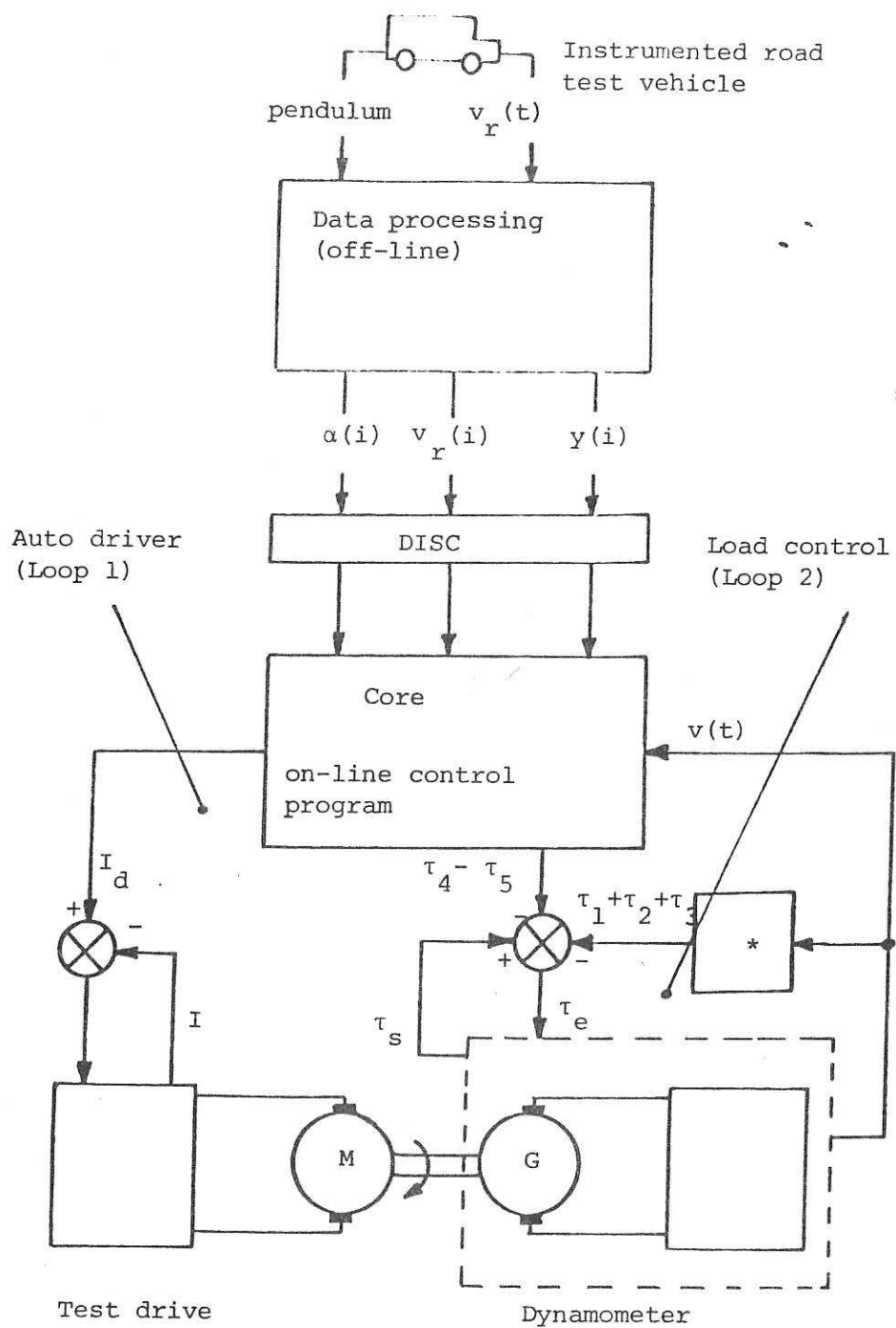with plug braking', Confidential report to Chloride Legg Ltd., Nov.1979.

8.   Acknowledgements
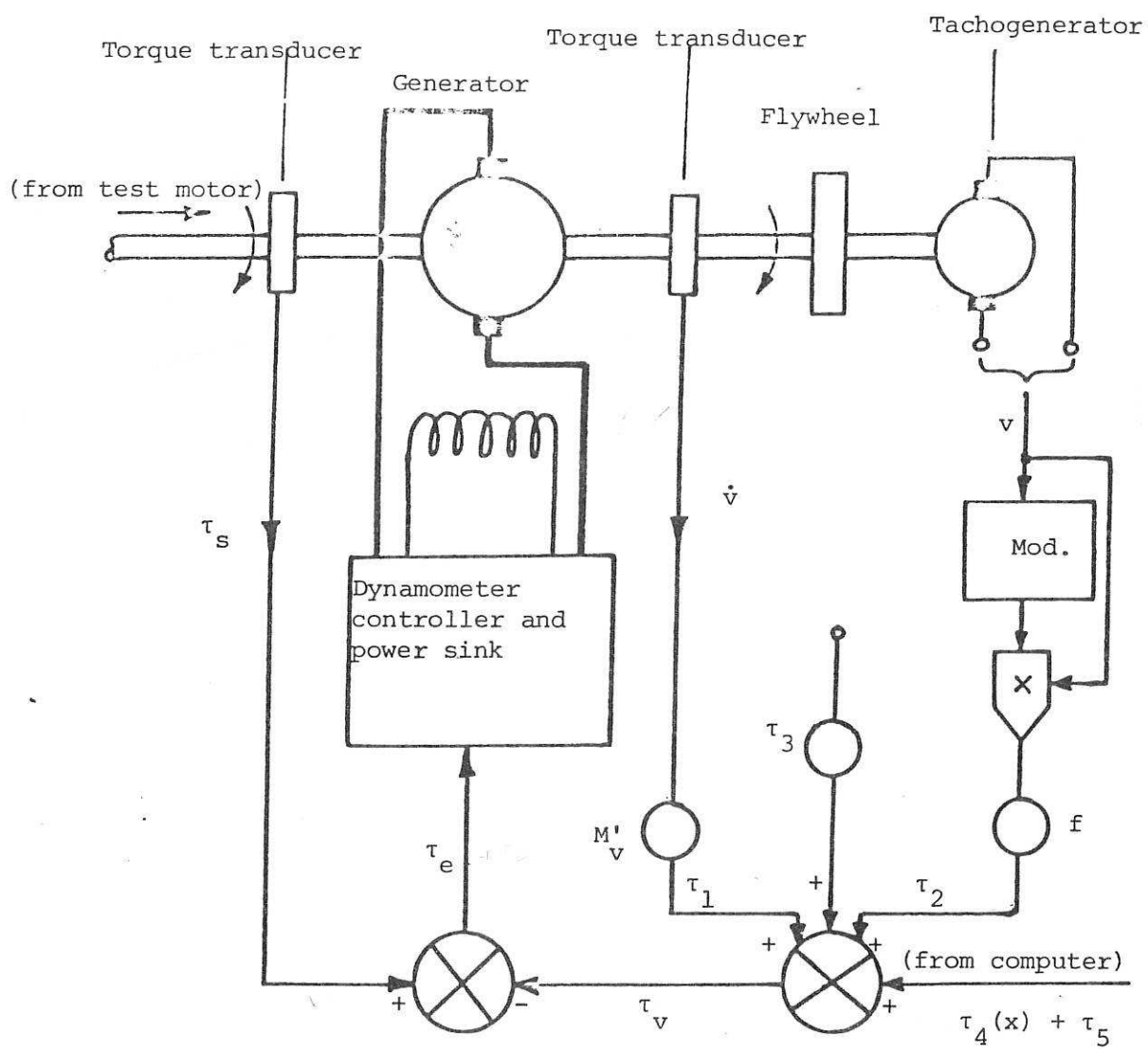
Fig. 1   Dynamometer and Local Controls

$$t = n\Delta T$$
set $i = n$
Read $v(n\Delta T)$
look-up $y(n)$ and $v_r(n)$

look up $\alpha(m)$

Table 1

i	$\alpha(i)$
o	$\alpha(o)$
1	$\alpha(1)$
m	$\alpha(m)$
n	$\alpha(n)$
N	$\alpha(N)$

*

Table 2

i	$v_r(i)$	$y(i)$
o	$v_r(o)$	$y(o)$
1	$v_r(1)$	$y(1)$
m	$v_r(m)$	$y(m)$
n	$v_r(n)$	$y(n)$
N	$v_r(N)$	$y(N)$

*

Set $\tau_4\{x(n)\} = W_v\alpha(m)$.
Calc. $I_d(t)$ and $\tau_5(t)$
from control laws.
Output I_d and $\tau_4 - \tau_5$.

Set $x_r(n) = y(n)$.
Set $x(n) = x(n-1)+v(n)\Delta T$.
Find m such that $y(m) = x(n)$.

* Table blocks which must be held in core when $t = n\,T$

Fig. 2 Control program flowchart

Instrumented road test vehicle

pendulum $v_r(t)$

Data processing
(off-line)

$\alpha(i)$ $v_r(i)$ $y(i)$

Auto driver
(Loop 1)

DISC

Load control
(Loop 2)

Core

on-line control
program

$v(t)$

I_d

$\tau_4 - \tau_5$

$\tau_1 + \tau_2 + \tau_3$

*

I

τ_s

τ_e

M   G

Test drive

Dynamometer

* Local loop transferred to computer in phase 2

Fig. 3 Showing role of computer in test arrangement

Speed (ft./s)

- - - - V_r
——— V

50

O   100   200   300   t(s)

Armature voltage

200

O   100   200   300   t(s)

Current (A)

- - - - Field current
——— armature current, I

800/30

100   200   300   t(s)
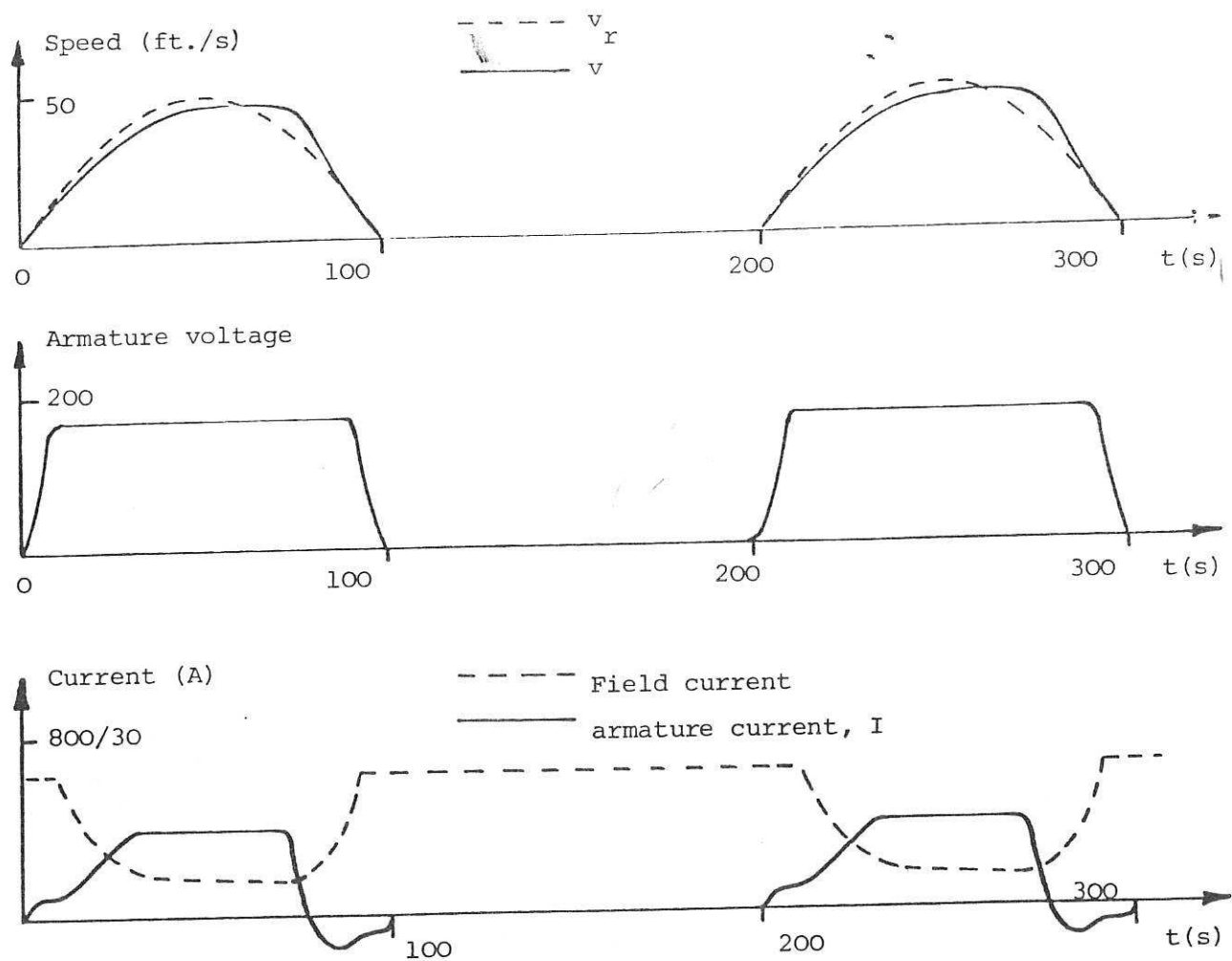
Fig. 4   Simulated performance of automatic driver
         (gradient 5% uphill)
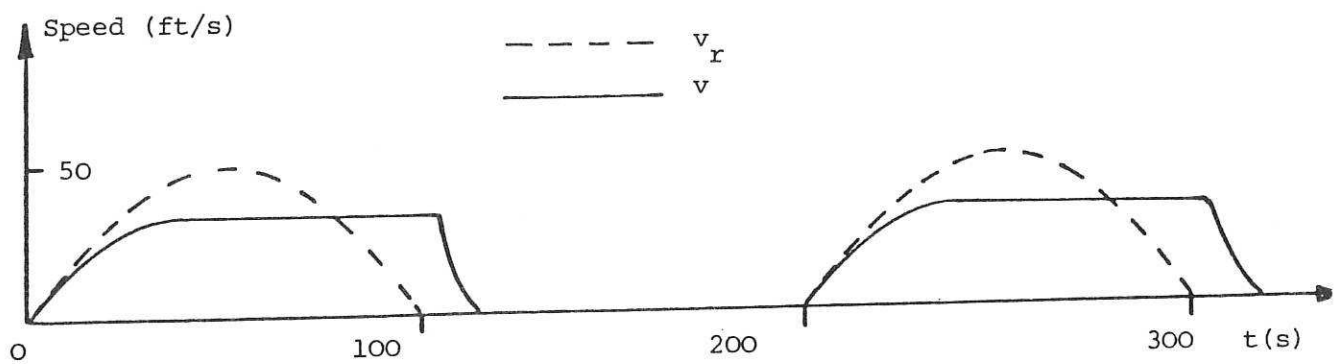
Fig. 5 Simulated performance on uphill gradient of 10%
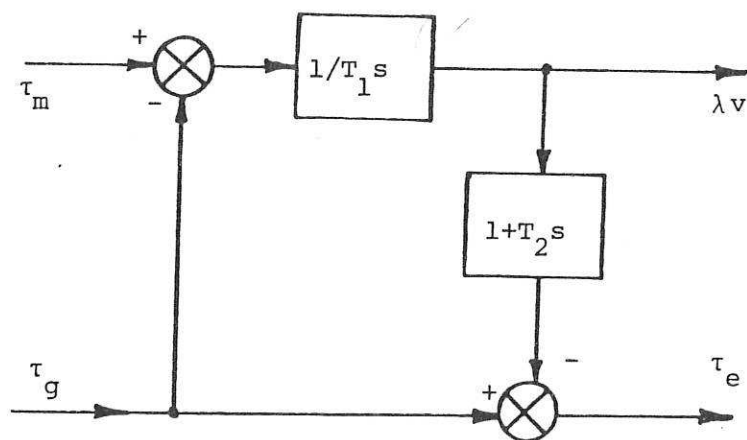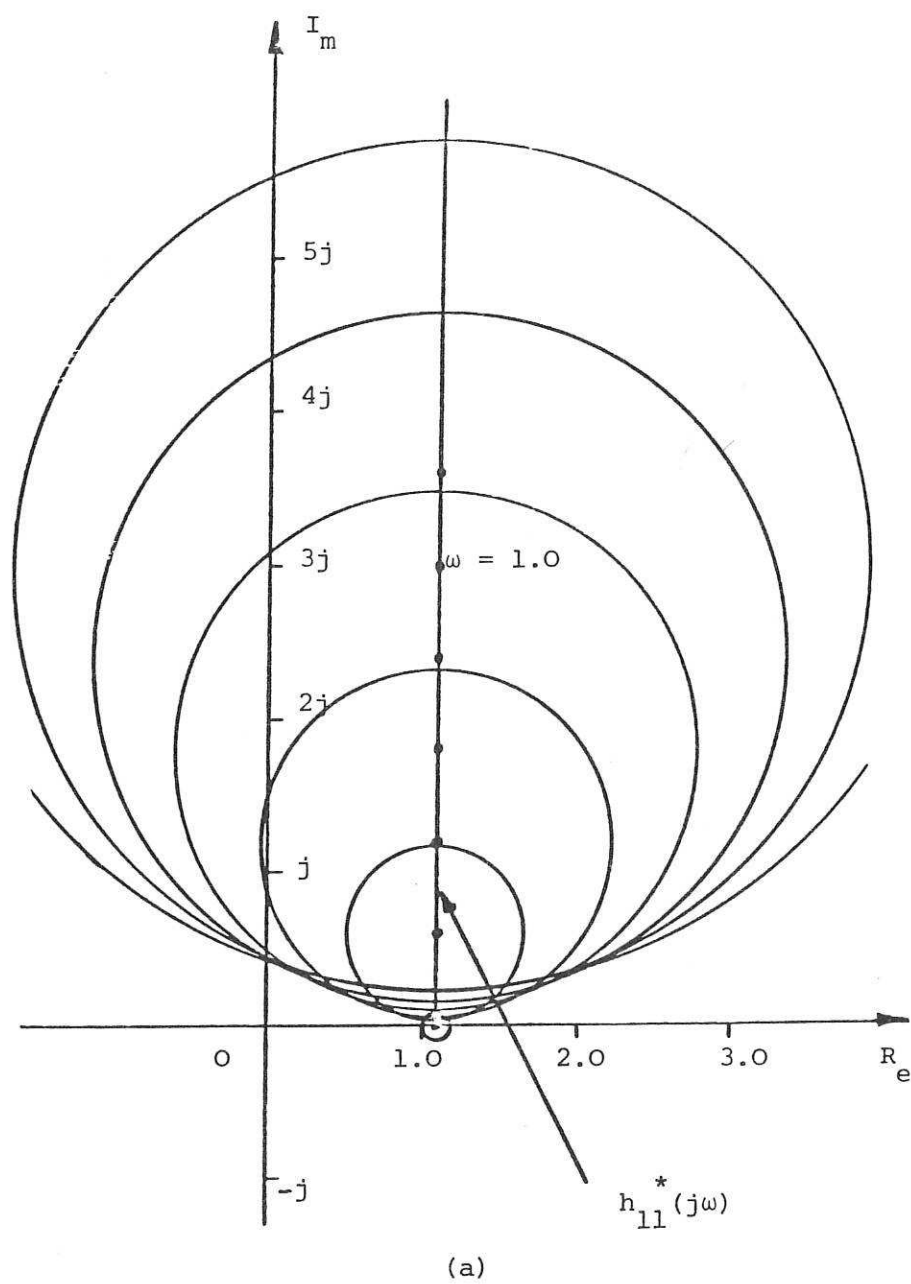
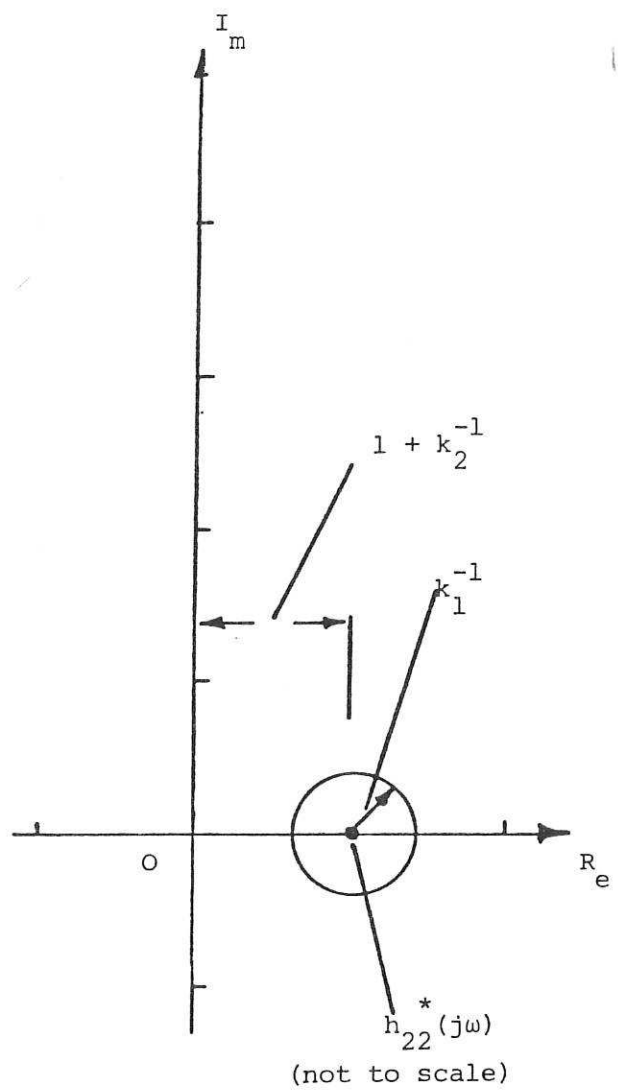Fig. 6   Open-loop block diagram
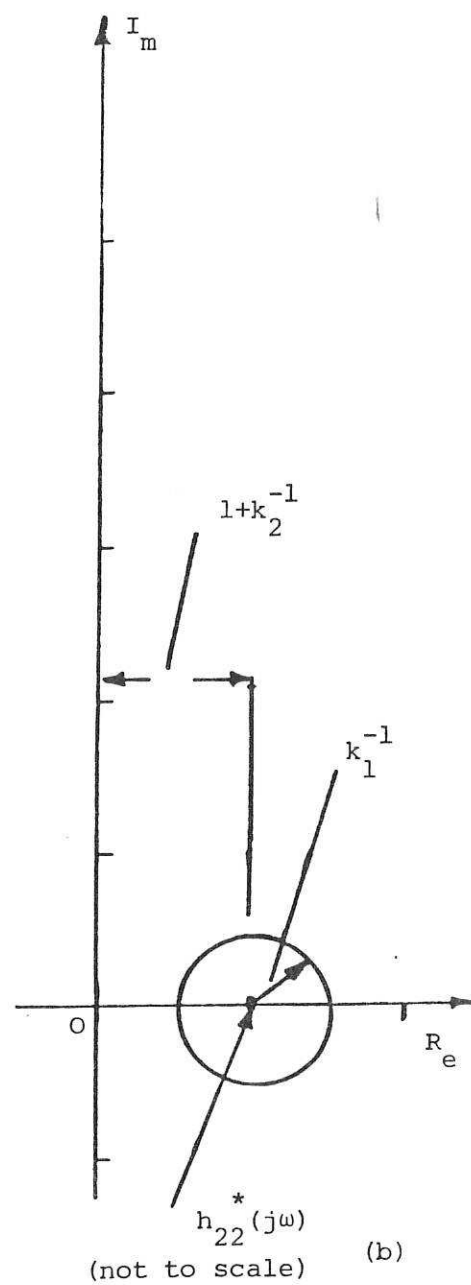
Fig. 7   Gershgorin bands for closed-loop system
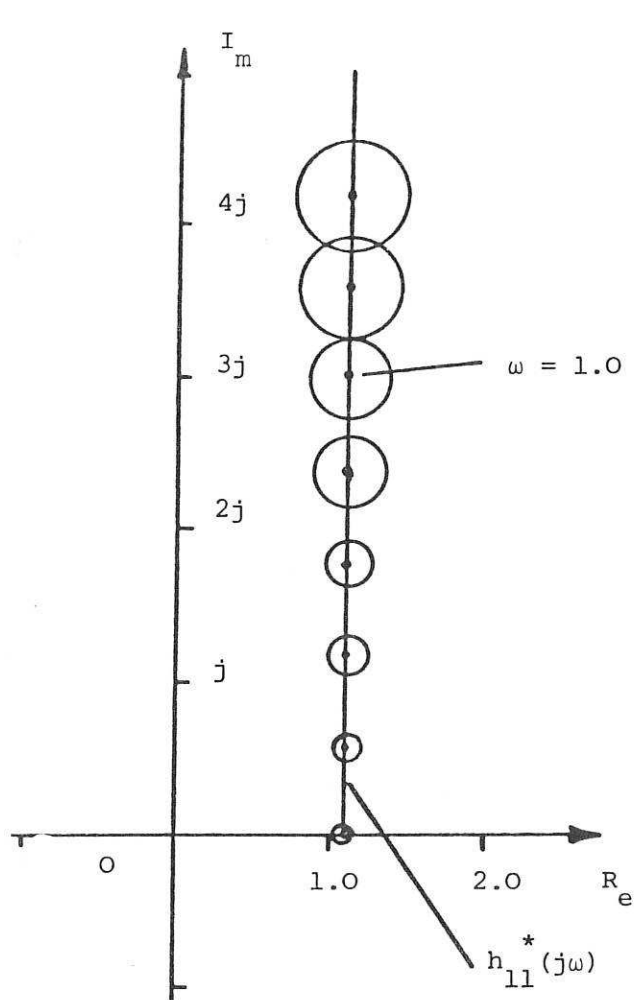
Fig. 8   <u>Ostrowski bands for closed loop system</u>
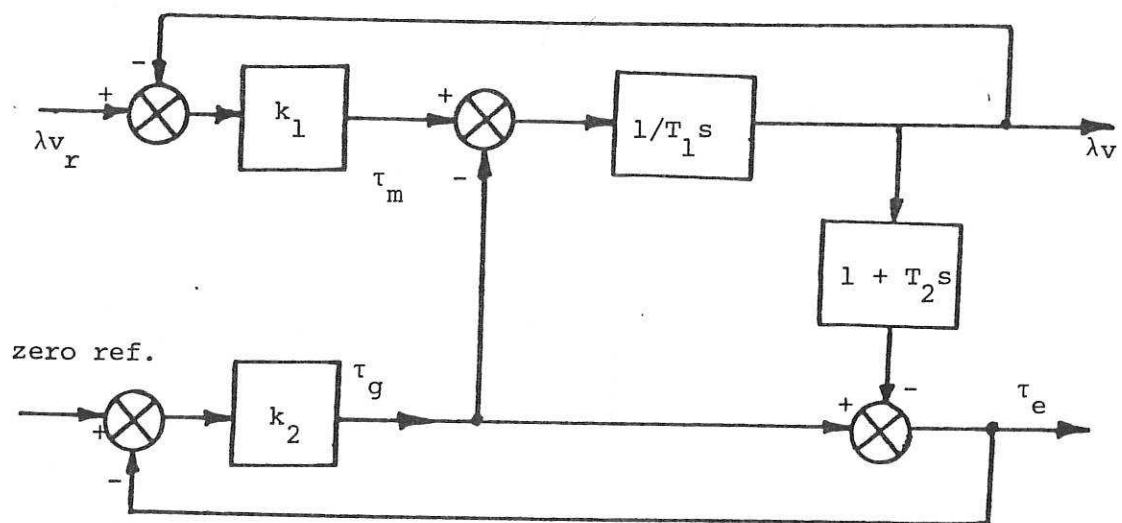
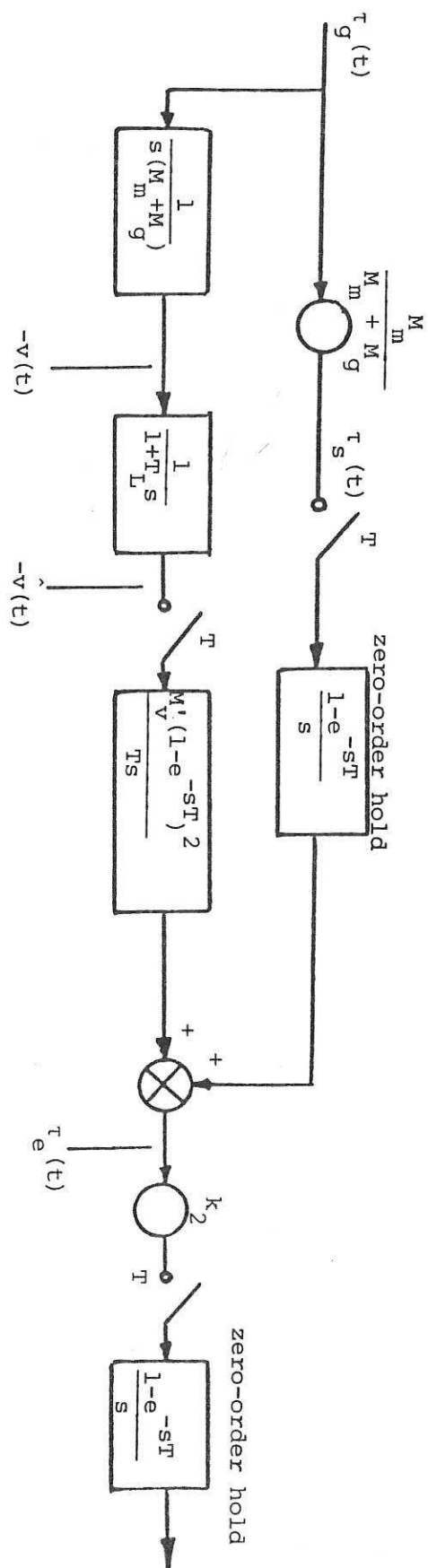Fig. 9   Closed-loop block diagram

Fig. 10   Block diagram for digital inertia simulation (open-loop)

Fig. 11 Comparison of rig and simulation
         performance (level road)